MNE 15 (2022) 100134

Contents lists available at ScienceDirect

Micro and Nano Engineering

journal homepage: www.sciencedirect.com/journal/micro-and-nano-engineering

AFM macro-probes to investigate whole 3D cardiac spheroids

Michele Zanetti [a,b,*], Laura Andolfi [a], Matthew R.G. Taylor [c], Luisa Mestroni [c], Marco Lazzarino [a]

[a] CNR-IOM, SS 14, km 163.5, Basovizza, Trieste, 34149, Italy
[b] University of Trieste, Department of Physics, Via Valerio 10, 34127 Trieste, Italy
[c] Molecular Genetics, Cardiovascular Institute, University of Colorado Denver, Anschutz Medical Campus, Aurora, CO 80045-2507, USA

ARTICLE INFO

Keywords:
AFM
Microfabrication
Cardiomyocytes
Spheroids
Rheology
Mechanobiology

ABSTRACT

In its many applications, the Atomic Force Microscope (AFM) is a promising tool in cardiac mechanobiology because it can unravel the viscoelastic and mechano-dynamic properties of individual cardiomyocytes. However, the biophysical investigation of more accurate 3D models is hampered by commercial probes, which typically operate at the cell sub-compartmental resolution. We have previously shown how flat macro-probes can overcome these limitations by extending the AFM mechanical measurements to multicellular aggregates. Such macro-probes are fabricated by standard micromachining and carry a flat polymeric wedge to offset the AFM mounting tilt. Therefore, the AFM is upgraded to a micro-parallel plate rheometer with unmatched force range and sensitivity. In this article, we show how these macro-probes can be applied to reveal the global rheology of primary cardiomyocytes spheroids, by performing stress-relaxation tests. More importantly, we demonstrate that these macro-probes can be used as passive sensors capable of monitoring the spheroid beating force and beating pattern, and to perform a "micro-CPR" on the spheroid itself.

1. Introduction

Cardiovascular diseases (CVDs) are the leading cause of death worldwide, according to the World Health Organization. A major problem in the recovery of infarcted patients is the inability of their hearts to rebuild a functioning syncytium. Instead, the contractile tissue is replaced by a fibrotic scar, leading to inadequate electromechanical compliance. Many efforts are being taken to tackle this epidemic. In recent years, studying the mechanical properties of the myocardium has become an imperative task that biophysicists must face to build accurate disease prediction models, regeneration strategies, and drug screening and testing tools. The Atomic Force Microscope (AFM) allows unraveling the mechano-dynamic behavior of single or clustered Cardiomyocytes (CMs) by quantifying their exerted beating force and profile down to the nanoscale [1,2], and their viscoelastic properties can be probed by AFM nanoindentation [3,4]. Since these properties usually reflect the molecular state of the cell, and generally its health, the AFM could evolve into an excellent in-vitro tool for drug screening and testing. Indeed, some papers present the AFM as a tool to provide useful information on the effects of a variety of substances on cardiac cells [5]. For example, when an inotropic agent (such as dopamine) is administered to a 2D cardiomyocyte culture, it alters its beating force. This force can be quantified by placing a sharp probe on the cell surface and monitoring its vertical deflection. Similarly, a "mechanocardiogram" (MCG) may show the effects of a chronotropic drug (such as caffeine), including a change in beating frequency, all at the single-cell level [6]. Moreover, AFM force spectroscopy (AFM-FS) is a gold standard to measure the mechanical properties of individual cells. In the framework of cardiac mechanobiology, nanoindentation studies were able to link a decrease in cell stiffness and adhesion to genetic variants in the lamin A/C gene (LMNA), responsible for the dilated and arrhythmogenic cardiomyopathies [7,8].

At the same time, a great deal of interest has been focused on creating more accurate in-vitro constructs of cardiac physiology and disease. Among them, Cardiac Spheroids (CSs) are promising three-dimensional (3D) models [9]. These constructs are built from primary [10] or iPSC-derived cardiomyocytes [11] which assemble to a spherical-like shape. Also, their cell population can be tuned according to the composition of the biological tissue by including other phenotypes, such as cardiac fibroblasts and/or endothelial cells [12]. These models allow to investigate the myocardium behavior within a richer and native environment and are valuable building blocks to bioprint complex microtissues with higher complexity [13,14].

Some studies have already shown the importance of assessing the

* Corresponding author.
E-mail address: zanetti@iom.cnr.it (M. Zanetti).

https://doi.org/10.1016/j.mne.2022.100134
Received 21 November 2021; Received in revised form 20 March 2022; Accepted 29 March 2022
Available online 1 April 2022

mechanical properties of CSs. For example, to measure their contractile force, they can be embedded into silicon rubbers whose deflection can be quantified and their action potentials analyzed by fluorescent calcium or potentiometric imaging [15].

However, to have a rigorous estimation of their global mechanical properties such as elasticity, viscosity, and plasticity, we need to consider what has already been developed for similar purposes, but on spheroids made of other cell types. In this regard, we refer to a recent review from Robert C. Boot [16] in which several physical methods are illustrated. Such methods comprise AFM local indentation [17], micropipette aspiration [18], micro-tweezers [19], spheroid fusion [20], and tissue surface tensiometry (TST) [21]. More recently, parallel plate compression has been proposed as a technique able to quantify the viscoelastic properties of living tissues [22]. In parallel plate rheology, a vertical loading of a rigid microplate allows the application of a uniaxial deformation to a spheroid, which is optically monitored by a camera. In this method, as for micropipette aspiration, the main issue is that they both rely on the visual microscopic assessment of the load ratio and, as result, they lack the force sensitivity required to accurately describe relevant phenomena such as small beating force variations.

To address this issue, we have developed AFM-compatible macro-probes that combine the AFM sensitivity with the advantages of parallel plate compression: with such an approach, oocytes deformations were successfully investigated [23], as well as multiple cell-cell interactions on large areas [24]. With this AFM-based system, the viscous contribution can be assessed by measuring the time of relaxation after sudden stress. During stress relaxation (SR), the whole spheroid is uniaxially compressed between two plates. Its displacement can be finely tuned by acting on the AFM piezoelectric actuator. Finally, its z-feedback loop is exploited to hold the position for long time intervals on the order of tens of seconds, minutes, or more. A Force-vs-Time curve is recorded and analyzed accordingly.

The purpose of this SR experiment is to demonstrate that, by using our AFM parallel macro-probes, it is possible to obtain relevant data regarding the viscoelastic behavior of whole cardiac spheroids and, by extension, of the myocardium itself. To our knowledge, this kind of evidence had not been disclosed yet because of the lack of a direct, and quantitative, physical technique.

More importantly, the macro-probes find their ultimate application in the field of mechanical stimulation. It is now generally accepted that external aids play a fundamental role in cardiomyocyte development. Mechanical stimulation increases matureness by activating hypertrophic pathways, while electrical stimulation improves connections and calcium handling [25]. On this matter, in this article, we also show how these macro-probes can be used to stimulate and monitor CSs contractility in real-time as if we are doing a “micro” heart massage.

2. Methods

2.1. Macro-probes fabrication

Different geometries and materials were evaluated using finite element analysis on COMSOL Multiphysics®, to achieve a suitable compromise between strength and sensitivity of the cantilever and to match the geometrical constraints imposed by large biological samples. Considering the size of multicellular spheroids (ranging from 100 to 400 μm), we developed a suspended Si_3N_4 cantilever of 300 × 300 μm in a square area, connected to the chip bulk through a pair of 100 × 100 μm arms. These arms are crucial in defining the stiffness of our system, as they sustain the stress induced by the cantilever deflection. The theoretical spring constant of such probes is ~4 N/m as calculated from COMSOL simulations.

The fabrication workflow, as already described in [23], consists of a combination of UV photolithography and dry/wet etching procedures. Those steps have been performed at the Nanofabrication Facility of Friuli Venezia Giulia (FNF, https://fnf.iom.cnr.it).

We begin by sputtering a thin layer (100 nm) of Cr on both sides of a 2 μm low-stress Si_3N_4-covered silicon wafer using a custom-built magnetron sputter-coater. The wafer surfaces were previously cleaned and activated in Piranha solution (30% H_2O_2 in 96% H_2SO_4 3:7). The pattern is transferred on the Cr-coated wafer using UV photolithography: MEGAPOSIT™ SPR™ 220 1.2 (Micro Resist GmbH) is spin-coated at 3000 rpm for 1′ on both sides of the wafer, which is later baked at 115 °C for 1′30″ on a generic hotplate. The following double-sided exposure under 375 nm UV light - by means of a MA25 mask aligner (Karl Suss KG) - make the exposed areas soluble in MF-24A solvent (Micro Resist GmbH).

After development, the exposed Cr is selectively etched away using an Ammonium Cerium nitrate/Acetic acid/H2O 6/1.1/18 solution. The sample is subjected to Reactive Ion Etching (RIE) for 1 h in a mixture of O_2/CF_4 plasma sustained by a DC bias of 100 W to expose the silicon beneath. A subsequent wet etching, performed in heated (80 °C) and stirred KOH solution (6.9 M), opens those areas, leaving the chips suspended and connected by structural branches. A thin (25 nm) layer of Au is finally evaporated onto the top side of the wafer to improve laser reflection on the AFM photodiode.

2.2. Macro-probes polymeric wedging

In almost every AFM setup, the cantilever hangs tilted from 10° to 20° to prevent any possible chip crash on the uneven sample surface. Considering the shape of our macro-probes, the above-mentioned pitch would hinder the application of a uniaxial loading, hence promoting indentation rather than uniform compression or inducing uncontrolled spheroid deformation and shifting during measurements. To provide a parallel and uniform compressing surface, we fabricate a polymeric wedge under the cantilever’s active area following the already described protocol by Steward and co-workers. [26]

We set up an optical path on an aluminum optical breadboard (Thorlabs), which is shown in Fig. 1-II. The setup consists of three main components: a 375 nm laser (not shown) which allows a rapid polymerization of the glue, a polymerization stage made of top and bottom plates (Fig. 1-II. a,b), and an optical assembly made of a 20× LWD lens (Olympus) coupled with a CMOS sensor (Thorlabs® 1625) for magnified observation (Fig. 1-II-c). Once the cantilever is punched out of its fabrication frame, it can be fixed to the appropriate AFM probe holder. The holder should always match the geometry of the available AFM since every instrument has its own mounting tilt. In our case, we employed a spare glass holder from JPK Instruments AG. Afterwards, the holder is secured to the top plate, whose vertical displacement can be adjusted using a single-axis translation stage driven by an amplified piezo motor (Thorlabs® TPZ001). Therefore, the Z position can be controlled in a standardized manner, which is necessary to fabricate reproducible wedges over a batch of macro-probes.

A tiny (about 10 uL) drop of a photopolymerizable glue (NOA 63) is deposited on a polydimethylsiloxane (PDMS, Sylgard 184, 1:10) membrane. Such membrane had been previously silanized to boost its hydrophobicity and ease the detachment of the glue after polymerization. The membrane is then placed on the stage’s bottom plate and the glue is localized under the cantilever by focusing on the lens field. While inspecting the camera, the motorized *Z*-stage is lowered, and the probe is brought into contact with the glue. After 5 s, the cantilever is lifted, and the fished glue is again pressed on a membrane’s free area, where the wedge is polymerized by the UV laser for 5 min. To avoid any breakage when lifting the probe from the PDMS, the stage is retracted at a slow speed of ~5 μm/s until complete separation. An additional 2′ UV exposure further hardens the glue. The elastic modulus of cured NOA73 is 11 MPa, which is thousands of times stiffer than that observed on multicellular systems. Therefore, it can be assumed to be infinitely rigid for our purposes.

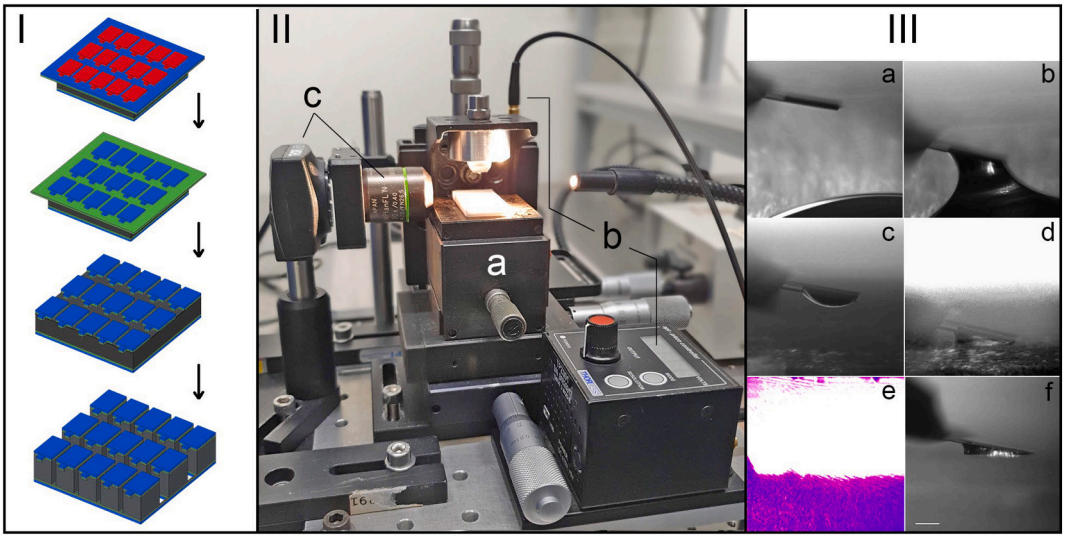

Fig. 1. (**I**) Brief scheme of a 3D section of the wafer undergoing progressive etching, after patterning. (**II**) Picture of the wedging setup highlighting the z-stage mount (**a**), the piezo-driven vertical positioning system (**b**), and the lens/camera assembly (**c**). (**III**) micrographs of the actual wedging procedure as taken from camera assembly, showing (**a**) cantilever's approach, (**b**) glue fishing, (**c**) fished drop, (**d**) wedge pre-formation on PDMS, (**e**) UV exposure, (**f**) polymerized wedge. Scalebar: 100 μm.

2.3. Macro-probes calibration

We calibrate our macro-probes via the spring-to-spring method [27] using a reference spring, a PPP-FM cantilever from Nanosensors®, with a known spring constant K_R = 2.15 N/m measured by thermal noise method. We start by mounting our chip on the AFM glass cube and positioning the laser spot on its center. Then, a series of voltage/distance curves are taken by pressing the macro-probe onto a glass surface, extrapolating the ratio between the laser deflection (as voltage variation) caused by the associated piezo excursion. The linear fit of the curve after the contact point leads to its slope, that is, the Absolute Sensitivity of the macro probe (S_0). We repeat the exact measurement pressing the probe onto the reference cantilever end, obtaining a Relative Sensitivity (S_R) proportional to the concomitant deflection of the reference.

The spring constants (K) of the macro probes are computed according to the equation:

$$K = K_R \bullet \left(\frac{S_R}{S_0} - 1\right)$$

2.4. Primary cardiomyocytes extraction

Post-natal day 3 (P3) Wistar rats are euthanized by decapitation and their chest cavity exposed by surgical incision. Ventricular Myocytes (NRVMs) are isolated following a well-established protocol [28–30] with minor modifications. Extractions mostly yield ~0.4 M viable NRVMs per heart. Briefly, hearts are pulled from the aorta and placed in a 50 mL centrifuge tube containing ice-cold CBFHH (Calcium and Bicarbonate-free Hank's buffer with Hepes) supplemented with Penicillin (50 U/mL) / Streptomycin (50 μg/mL) and Heparin (Sigma® H3149 at 2 U/mL). Each heart is aseptically minced using surgical scissors, attaining regularly sized fragments of ~1 mm. Tissue is digested at RT in the same buffer supplemented with Trypsin (Sigma® T4799 at 0.70 mg/mL) and DNAse I (Roche AG at 25 U/mL), to limit cell clumping, over 3 h. The cell suspension is then centrifuged (300 RCF, 10′), the supernatant discarded, and the pellet resuspended in fresh growth media (Sigma® M0643 MEM supplemented with 5% Calf Serum, 0.2% Penicillin-Vitamin B12). Fibroblasts are removed by pre-plating for 45′ into 2× T75 flasks. Finally, enriched NRVMs are collected from the flasks' supernatant, centrifuged again (100 RCF, 5′), and resuspended at a density of 2.5 M/mL in fresh media.

2.5. 3D cardiac spheroids plating

Cardiac Spheroids (CS) are formed via the hanging drop method [31] starting from the 2.5 M/mL single-cell suspension. For this purpose, a 96 mm ø polystyrene Petri dish is flipped upside down. Twenty drops of 20 μL each of cell suspension are pipetted on the inner lid, resulting in ~50 k cells per drop. The bottom plate is then filled with sterile water, and the lid is flipped onto it, leaving the drops hanging. CS assemble over three days of incubation at 95% H_2O, 5% CO2, 37 °C atmosphere.

2.6. AFM measurement setup

The wedged and calibrated probe is mounted to the side-view cantilever holder of a JPK NanoWizard® II AFM. We choose such a holder as it bears an inclined mirror on the cantilever forefront, allowing us to look at the spheroid deformation from the aside. However, this implies the need to perform these measurements on the edge of a stepped surface to avoid mirror crashing. For this purpose, a set of 24 mm ø glass coverslips are spin-coated with the PDMS premix at 2000 rpm and cured overnight in a ventilated oven at 70 °C. To obtain a suspended platform, we use NOA73 optical adhesive (Norland Products, Inc.) to glue a cleaved piece of microscope slide inside a 35 mm ø Petri dish cover. On top, we glue the PDMS-coated coverslip in such a way that roughly half of it protrudes towards the center of the Petri. The hanging platform is finally positioned on the JPK CellHesion® module, which enables an extended z-piezo excursion of 100 μm. This measurements setup is represented in Fig. 4, panels B/C.

2.7. Cardiac spheroids stress-relaxation (SR)

At the fourth incubation day, each spheroid has a diameter ranging from 300 to 400 μm (Fig. 4-A). After its retrieval, a 10 μL drop of Hank's Buffer with Hepes (HHBS) is placed on the edge of the PDMS coverslip and the spheroid is rapidly transferred inside it. Thanks to the surface hydrophobicity, the CS remains confined and is rapidly localized. Then, the CS is approached with the probe and wait for a weak adhesion to set in. After about 1 min, the probe is slightly lifted (5 μm) from the surface, along with the fished CS. Finally, we carefully fill the Petri lid with warm HHBS while the spheroid hangs from the probe.

To start the SR, the stage is lifted by 30 μm (500 ms) towards the cantilever, so the spheroid becomes suddenly compressed. Then, the

piezo is locked in position. By monitoring the vertical deflection over time, it is possible to follow the relaxation pattern of the spheroid quantitatively because the cantilever had been previously calibrated against a reference probe. The test is performed on three spheroids (SPH1/2/3) by collecting 10 to 12 curves each, with 5″ pauses in-between. Then, each Force vs Time curve is analyzed by fitting the data to a two-component Maxwell model by least-square method. The model is described by the following equation:

$$F(t) = a_0 + a_1 \bullet e^{-\frac{t-t_0}{\tau_1}} + a_2 \bullet e^{-\frac{t-t_0}{\tau_2}}$$

The model considers an initial, elastic response and a following viscous relaxation. Therefore, each CSs is approximated to a pure viscoelastic body whose relaxation occurs in a set of times, τ1 and τ2, where:

$$\tau = \frac{\eta}{E}$$

i.e., the ratio between the viscous and the elastic components. The fitting procedure is performed on Igor Pro (Wavemetrics Inc.), and finally, values are mediated for each CS.

3. Results and discussion

The micromachining process resulted in a series of probes batch suspended from a silicon frame via connecting arms (Fig. 2-A).

The fabrication met the physical requirements, although there was an undesirable over/under etching of the silicon at the end of the chip, opposite to the cantilever side. This can be seen in Fig. 2-A where black regions are silicon while the yellow ones are gold-coated silicon nitride membranes. However, if mounted properly, this defect does not affect operation. In attempting to solve this minor problem, a slight redesign of the optical masks might be considered.

Regarding the polymeric wedge, SEM imaging (Fig. 3) shows the detachment pattern of the hardened NOA73 resin, represented by transverse lines. This can result from the separation of the surfaces (i.e., the resin and the PDSM) occurring in discrete steps rather than continuously. One way to minimize this effect would be to extend the curing time, but this could strengthen the bond between the adhesive and PDMS, making them harder to separate, to the point of fracturing the Si_3N_4 arms. Nevertheless, this microscopic pattern does not affect the performance of the measurements because the lines are narrow, and the roughness lies in the order of hundreds of nanometers. Larger detachment lines could have caused multiple indentations instead of a uniform compression, which is why it is important to fabricate a smooth surface.

After the calibration, we determined the macro-probe spring constant to be K = 1.67 N/m.

Regarding SR measurements, three CS were initially probed (SPH1, SPH2, and SPH3) using this calibrated probe. After the sudden (500 ms) 30 μm deformation induced by the piezo-driven displacement towards the probe, the closed feedback loop of the AFM was exploited to hold the position for 30 s. The corresponding stress, as shown in Fig. 5-B, is about 7 μN per each CS. As a result, the CS recovered from the applied stress in a double exponential decay. All the spheroids showed a similar relaxation pattern consisting of a rapid elastic relaxation followed by a slow viscous dissipation (see Fig. 5-B) rather than a single exponential decay. This phenomenon is known from studies on other microtissues and has already been discussed in a pioneering work carried out via micropipette aspiration [18].

Two relaxation constants (τ1 and τ2) are extrapolated by least-square fitting. The exemplificative distribution is shown in Fig. 5-C. The first relaxation (τ1) occurs in a time of (0.747 ± 0.153) s, (0.521 ± 0.056) s, (0.685 ± 0.073) s for SPH1, SPH2, and SPH3 respectively (Mean ± SD). The second relaxation occurs in a time (τ2) of (9.22 ± 1.45) s, (9.26 ± 0.61) s, (9.59 ± 0.57) s. Both τ1 and τ2 show a SD less then 11%, apart from SPH1 for which it is higher (20% and 16%). As seen from the optical micrographs in Fig. 4-A, SPH1 appears to be slightly larger than the other two, while its external corona is less compact. It can be hypothesized that the mechanical interactions between the embedded cells differ from the other spheroids because of its apparent looser architecture, resulting in relaxation times which in turn are more dispersed. Moreover, the compression section of the SR plots (Fig. 5-B first 500 ms of red curves) tells us SPH1 is softer because of the reduced slope, which agrees with the optical evaluation and the higher relaxation times.

Interestingly, in the beginning, CS did not spontaneously contract. However, they started to, after a few SR cycles (see Fig. 6-A). This finding is consistent with the concept of the heart mechano-electric feedback, which tells an electrical current leads to a contraction, but the opposite is also true, giving rise to a feedback loop thanks to which a forced contraction often induces an autonomous one [32]. In a recent work [33], the same effect was observed on human-derived self-beating spheroids. Nakano and co-workers were able to uniaxially compress individuals and pairs of CSs and monitor their electromechanical coupling under parallel plates, via creep measurements. They also showed how CS work both under and against mechanical load, and how their beating frequency is influenced by the applied static force. The upper plate of their system was connected to a calibrated spring whose compression was monitored by optical microscopy. We reproduced Nakano's experiment on our spheroids using our macro-cantilevers which offer, thanks to the AFM configuration, a much better force and position sensitivity and faster time responses. Instead of creep experiments, we applied a set of mechanical stimulations via the AFM macro-probe to the CSs. By inducing 10 cyclic compressions (650 ms, 50 μm displacement setpoint), we could induce a transient beating and, at the same time, evaluate the beating pattern. Graphics in Fig. 6-B represent an example of this experiment performed on SPH1 after the SR. The

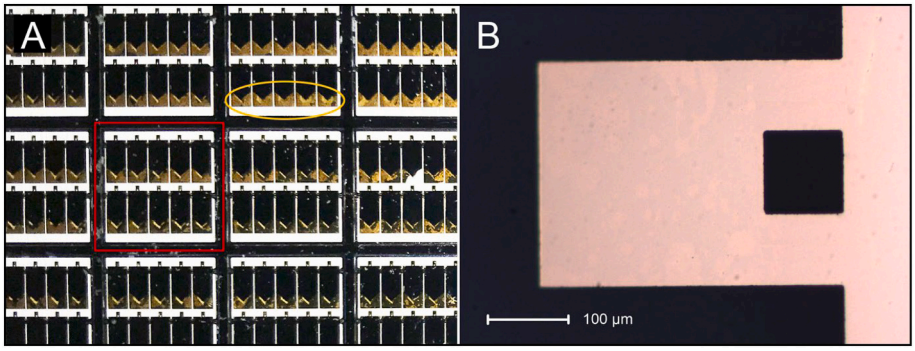

Fig. 2. A. central section of the processed silicon nitride wafer. A single element is made by 10 individual chips (red square). The opposite end from the macro-probe (yellow circle) displays unwanted silicon etching. **B**, an optical micrograph of the suspended macro-probe prior to wedging. (For interpretation of the references to colour in this figure legend, the reader is referred to the web version of this article.)

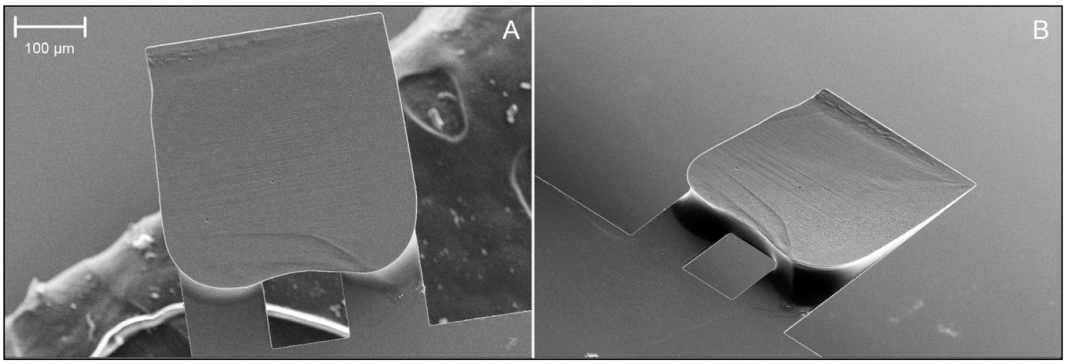

Fig. 3. SEM micrographs of the bottom side of the probe after its polymeric wedging. Small imperfections can be observed, especially from a tilted angle (**right**).

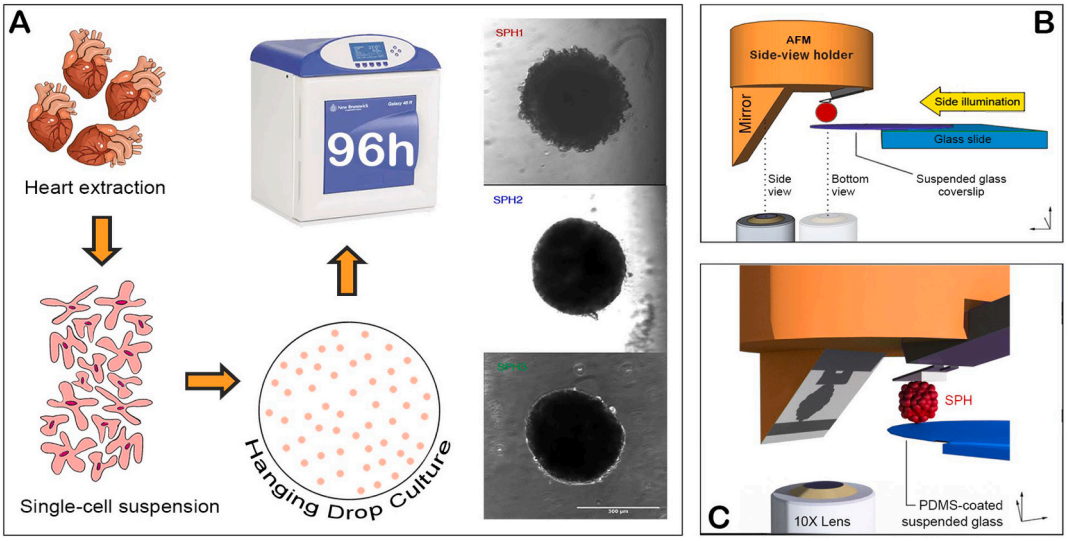

Fig. 4. A. Scheme of the CSs plating. SPH1/2/3 are shown on its right as taken from the inverted microscope before the actual measurement. Notice how SPH1 displays an irregular cell corona. **B/C.** CAD renders (Adobe® Photoshop 3D) of the JPK NanoWizard® II in side-view configuration. Detail **(C)** shows a computed ray-traced projection of the side-view as reflected by the suspended mirror.

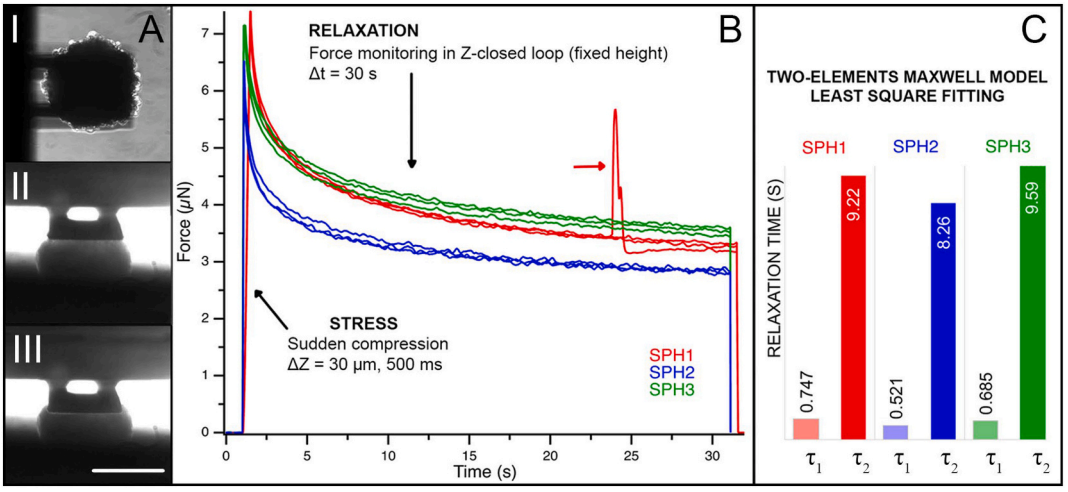

Fig. 5. A. Optical images of a CS under a macro-cantilever. **(a)** Bottom-view. **(b)** Side-view imaging before compression **(c)** After compression. Scalebar: 300 µm. **B**: nine stress-relaxation curves as obtained through the AFM, after baseline subtraction. The samples (SPH1/2/3) showed similar relaxation patterns. SPH1 shows contractility (red arrow) at ~25 s. A fast (τ1) and slow (τ2) relaxation regimens were obtained during fitting procedure (**C**). (For interpretation of the references to colour in this figure legend, the reader is referred to the web version of this article.)

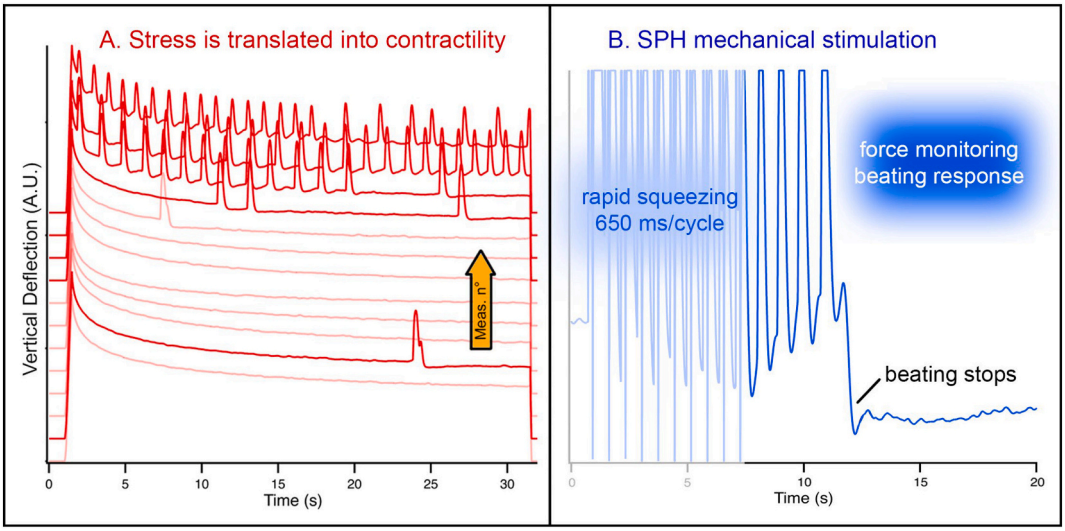

Fig. 6. A. Inactive spheroids started beating after a few SR cycles translating a mechanical stimulus to autonomous contractility. Yellow arrow indicates progressiveness in measurement number (from 1 to 12, for SPH1). Each curve is vertically displaced by 1 A.U. to discriminate the single measurement. **B** shows the effects of a controlled stimulation on SPH1, resulting into transient contractility from ~7 to ~12 s. (For interpretation of the references to colour in this figure legend, the reader is referred to the web version of this article.)

faded portion of the plot (first ~7 s) shows the cyclic compressions, while the rest of the plot shows the passive force monitoring of the CS transient beating, i.e., the vertical deflection of the cantilever over time, while the CS is displacing it upwards by its contractions. After 4–5 contractions, SPH1 stopped beating and needed another cycle of micro-CPR to beat again, probably because the cardiomyocytes had already reached a significant maturation level at P3 (plus 4 days in culture). Since our probes' spring constant is known, we could also have performed the mechanical loading using a force setpoint instead of a z-displacement one. We regard this as a prominent detail since it would allow investigating the CS response at different loading forces. We refer to this kind of experiment as "micro-CPR" because of the analogy to the human cardiopulmonary resuscitation applied as chest compressions.

Our platform could greatly help explore the results of prolonged mechanical stimulation on the CS development, albeit we should consider the need for a biological environment for the CSs to survive for a long time. For this purpose, a redesign of the macro-probe would be essential to be fully integrated - for example - into a cell culture incubator. In this framework, its operation would have to be decoupled from the AFM machine, e.g., by integrating a piezoelectric circuit on its legs as a sensing element (to measure its deflection) and a piezoelectric tube as a displacement actuator (to tune its vertical load).

4. Conclusions

Mechanobiology of heart tissue is a rapidly growing field of research that holds important promises in numerous applications. The rising availability of three-dimensional constructs for heart tissue modeling could help create novel drug-testing platforms, further reducing the gap between animal models and the human heart. Moreover, it opens new possibilities regarding the bio-fabrication of cardiac patches for infarcted tissue regeneration in personalized medicine. On another side, the AFM is a powerful tool to inspect these constructs' mechanical properties but is practically limited by their size, allowing a local nano-investigation only. For this reason, we have shown how it is possible to extend the AFM capabilities to the mechanical investigation of cardiac spheroids by fabricating flat macro-cantilevers. We have designed and later performed their micromachining in a cleanroom environment and showed their optical and SEM characterization. We have used these macro-probes to perform stress-relaxation measurements of whole cardiac spheroids made of primary neonatal rat cardiomyocytes. We were able to measure their beating force and frequency, and we stimulated their beating via the AFM itself via a so-called "micro-CPR". To our knowledge, this is the first time cardiac spheroids are individually probed and stimulated by such a sensitive instrument.

Supplementary data to this article can be found online at https://doi.org/10.1016/j.mne.2022.100134.

Ethical standards

The study was conducted according to the guidelines of the Declaration of Helsinki and approved by the OPBA Committee of the University of Trieste, under the Italian Ministry of Education, University, and Research (protocol code 1FF80.N.PZB).

Author contributions

Conceptualization: M.Z., M.L., M.R.G.T., L.M.; Data curation: M.Z.; Formal analysis: M.Z., M.L.; Funding acquisition: M.L.; Investigation: M.Z., L.A.; Supervision: M.L., L.A.; Writing - original draft: M.Z.; Writing - review & editing: M.Z., L.A., M.L., M.R.G.T., L.M.

Declaration of Competing Interest

The authors declare that they have no known competing financial interests or personal relationships that could have appeared to influence the work reported in this paper.

Acknowledgments

We acknowledge and thank the Italian Liver Foundation (Fondazione Italiana Fegato ONLUS, Trieste) for the donation of the excess animal tissues, an absolute prerequisite for the sustainability of our work. In particular, we thank Dr. Silvia Gazzin, Dr. Sri Yayanti and Prof. Claudio Tiribelli. In addition, we thank Dr. Brisa Marisol Pena Castellanos and Dr. Ilaria Pecorari for the precious help regarding the cardiomyocytes' isolation protocol, and its application. We finally acknowledge the University of Trieste and the Material's Foundry Institute CNR-IOM for the provided co-funding.

References

[1] J. Liu, N. Sun, M.A. Bruce, J.C. Wu, M.J. Butte, Atomic force mechanobiology of pluripotent stem cell-derived cardiomyocytes, PLoS One 7 (2012), https://doi.org/10.1371/journal.pone.0037559.

[2] G. Caluori, R. Raiteri, M. Tedesco, Simultaneous AFM investigation of the single cardiomyocyte electro-chemo-mechanics during excitation-contraction coupling, Methods Mol. Biol. 2019 (1886) 355–367, https://doi.org/10.1007/978-1-4939-8894-5_21.

[3] E.U. Azeloglu, K.D. Costa, Cross-bridge cycling gives rise to spatiotemporal heterogeneity of dynamic subcellular mechanics in cardiac myocytes probed with atomic force microscopy, Am. J. Physiol. Heart Circ. Physiol. 298 (2010), https://doi.org/10.1152/AJPHEART.00427.2009/SUPPL_FILE/VIDEO.

[4] A.B. Mathur, A.M. Collinsworth, W.M. Reichert, W.E. Kraus, G.A. Truskey, Endothelial, cardiac muscle and skeletal muscle exhibit different viscous and elastic properties as determined by atomic force microscopy, J. Biomech. 34 (2001) 1545–1553, https://doi.org/10.1016/S0021-9290(01)00149-X.

[5] D. Borin, I. Pecorari, B. Pena, O. Sbaizero, Novel insights into cardiomyocytes provided by atomic force microscopy, Semin. Cell Dev. Biol. 73 (2018) 4–12, https://doi.org/10.1016/j.semcdb.2017.07.003.

[6] M. Pesl, J. Pribyl, I. Acimovic, A. Vilotic, S. Jelinkova, A. Salykin, A. Lacampagne, P. Dvorak, A.C. Meli, P. Skladal, V. Rotrekl, Atomic force microscopy combined with human pluripotent stem cell derived cardiomyocytes for biomechanical sensing, Biosens. Bioelectron. 85 (2016) 751–757, https://doi.org/10.1016/J.BIOS.2016.05.073.

[7] E. Laurini, V. Martinelli, T. Lanzicher, L. Puzzi, D. Borin, S.N. Chen, C.S. Long, P. Lee, L. Mestroni, M.R.G. Taylor, O. Sbaizero, S. Pricl, Biomechanical defects and rescue of cardiomyocytes expressing pathologic nuclear lamins, Cardiovasc. Res. 114 (2018) 846–857, https://doi.org/10.1093/cvr/cvy040.

[8] T. Lanzicher, V. Martinelli, L. Puzzi, G. Del Favero, B. Codan, C.S. Long, L. Mestroni, M.R.G. Taylor, O. Sbaizero, The cardiomyopathy lamin A/C D192G mutation disrupts whole-cell biomechanics in cardiomyocytes as measured by atomic force microscopy loading-unloading curve analysis, Sci. Rep. 5 (2015) 1–14, https://doi.org/10.1038/srep13388.

[9] L. Polonchuk, M. Chabria, L. Badi, J.C. Hoflack, G. Figtree, M.J. Davies, C. Gentile, Cardiac spheroids as promising in vitro models to study the human heart microenvironment, Sci. Rep. 7 (2017), https://doi.org/10.1038/s41598-017-06385-8.

[10] R. Noguchi, K. Nakayama, M. Itoh, K. Kamohara, K. Furukawa, J.-I. Oyama, K. Node, S. Morita, Development of a three-dimensional pre-vascularized scaffold-free contractile cardiac patch for treating heart disease, J. Heart Lung Transplant. 35 (2016) 137–145, https://doi.org/10.1016/j.healun.2015.06.001.

[11] S. Mattapally, W. Zhu, V.G. Fast, L. Gao, C. Worley, R. Kannappan, A.V. Borovjagin, J. Zhang, Spheroids of cardiomyocytes derived from human-induced pluripotent stem cells improve recovery from myocardial injury in mice, Am. J. Physiol. Heart Circ. Physiol. 315 (2018) H327–H339, https://doi.org/10.1152/AJPHEART.00688.2017/SUPPL_FILE/SUPPLEMENTAL.

[12] P. Beauchamp, C.B. Jackson, L.C. Ozhathil, I. Agarkova, C.L. Galindo, D.B. Sawyer, T.M. Suter, C. Zuppinger, 3D co-culture of hiPSC-derived cardiomyocytes with cardiac fibroblasts improves tissue-like features of cardiac spheroids, Front. Mol. Biosci. 7 (2020) 14, https://doi.org/10.3389/FMOLB.2020.00014/BIBTEX.

[13] A.C. Daly, M.D. Davidson, J.A. Burdick, 3D bioprinting of high cell-density heterogeneous tissue models through spheroid fusion within self-healing hydrogels, Nat. Commun. 2021 121 (12) (2021) 1–13, https://doi.org/10.1038/s41467-021-21029-2.

[14] L. Polonchuk, L. Surija, M.H. Lee, P. Sharma, C.L.C. Ming, F. Richter, E. Ben-Sefer, M.A. Rad, H.M.S. Sarmast, W. Al Shamery, H.A. Tran, L. Vettori, F. Haeusermann, E.C. Filipe, J. Rnjak-Kovacina, T. Cox, J. Tipper, I. Kabakova, C. Gentile, Towards engineering heart tissues from bioprinted cardiac spheroids, Biofabrication. 13 (2021), https://doi.org/10.1088/1758-5090/AC14CA.

[15] K. Andrysiak, J. Stępniewski, J. Dulak, Human-induced pluripotent stem cell-derived cardiomyocytes, 3D cardiac structures, and heart-on-a-chip as tools for drug research, Pflugers Arch. - Eur. J. Physiol. 4737 (473 (2021)) (2021) 1061–1085, https://doi.org/10.1007/S00424-021-02536-Z.

[16] R.C. Boot, G.H. Koenderink, P.E. Boukany, Spheroid Mechanics and Implications for Cell Invasion 6, 2021, https://doi.org/10.1080/23746149.2021.1978316.

[17] V. Vyas, M. Solomon, G.G.M. D'Souza, B.D. Huey, Nanomechanical analysis of extracellular matrix and cells in multicellular spheroids, Cell. Mol. Bioeng. 12 (2019) 203–214, https://doi.org/10.1007/S12195-019-00577-0/FIGURES/6.

[18] K. Guevorkian, M.J. Colbert, M. Durth, S. Dufour, F. Brochard-Wyart, Aspiration of biological viscoelastic drops, Phys. Rev. Lett. (2010), https://doi.org/10.1103/PhysRevLett.104.218101.

[19] D. Jaiswal, N. Cowley, Z. Bian, G. Zheng, K.P. Claffey, K. Hoshino, Stiffness analysis of 3D spheroids using microtweezers, PLoS One 12 (2017), https://doi.org/10.1371/JOURNAL.PONE.0188346.

[20] N.V. Kosheleva, Y.M. Efremov, B.S. Shavkuta, I.M. Zurina, D. Zhang, Y. Zhang, N. V. Minaev, A.A. Gorkun, S. Wei, A.A. Shpichka, I.N. Saburina, P.S. Timashev, Cell spheroid fusion: beyond liquid drops model, Sci. Rep. 2020 101 10 (2020) 1–15, https://doi.org/10.1038/s41598-020-69540-8.

[21] A. Mgharbel, H. Delanoë-Ayari, J.P. Rieu, Measuring accurately liquid and tissue surface tension with a compression plate tensiometer 3 (2010) 213–221, https://doi.org/10.2976/1.3116822.

[22] R. Yanbarisov, Y. Efremov, N. Kosheleva, P. Timashev, Y. Vassilevski, Numerical modelling of multicellular spheroid compression: viscoelastic fluid vs. viscoelastic solid, Mathematics. 9 (2021), https://doi.org/10.3390/MATH9182333.

[23] L. Andolfi, S.L.M. Greco, D. Tierno, R. Chignola, M. Martinelli, E. Giolo, S. Luppi, I. Delfino, M. Zanetti, A. Battistella, G. Baldini, G. Ricci, M. Lazzarino, Planar AFM macro-probes to study the biomechanical properties of large cells and 3D cell spheroids, Acta Biomater. 94 (2019) 505–513, https://doi.org/10.1016/j.actbio.2019.05.072.

[24] M. Zanetti, S.N. Chen, M. Conti, M.R.G. Taylor, O. Sbaizero, L. Mestroni, M. Lazzarino, Microfabricated cantilevers for parallelized cell-cell adhesion measurements, Eur. Biophys. J. (2021), https://doi.org/10.1007/S00249-021-01563-Z.

[25] W.L. Stoppel, D.L. Kaplan, L.D. Black, Electrical and mechanical stimulation of cardiac cells and tissue constructs, Adv. Drug Deliv. Rev. 96 (2016) 135, https://doi.org/10.1016/J.ADDR.2015.07.009.

[26] M.P. Stewart, A.W. Hodel, A. Spielhofer, C.J. Cattin, D.J. Müller, J. Helenius, Wedged AFM-cantilevers for parallel plate cell mechanics, Methods. 60 (2013) 186–194, https://doi.org/10.1016/J.YMETH.2013.02.015.

[27] J.L. Hutter, J. Bechhoefer, Calibration of atomic-force microscope tips, Rev. Sci. Instrum. (1993), https://doi.org/10.1063/1.1143970.

[28] P. Simpson, S. Savion, Differentiation of rat myocytes in single cell cultures with and without proliferating nonmyocardial cells. Cross-striations, ultrastructure, and chronotropic response to isoproterenol, Circ. Res. 50 (1982) 101–116, https://doi.org/10.1161/01.RES.50.1.101.

[29] C.S. Long, K. Kariya, L. Karns, P.C. Simpson, Sympathetic modulation of the cardiac myocyte phenotype: studies with a cell-culture model of myocardial hypertrophy, Basic Res. Cardiol. 87 (Suppl. 2) (1992) 19–31, https://doi.org/10.1007/978-3-642-72477-0_3.

[30] V. Martinelli, G. Cellot, A. Fabbro, S. Bosi, L. Mestroni, L. Ballerini, Improving cardiac myocytes performance by carbon nanotubes platforms, Front. Physiol. 4 (SEP) (2013) 239, https://doi.org/10.3389/FPHYS.2013.00239/BIBTEX.

[31] R. Foty, A simple hanging drop cell culture protocol for generation of 3D spheroids, J. Vis. Exp. (2011), https://doi.org/10.3791/2720.

[32] P. Kohl, U. Ravens, Cardiac mechano-electric feedback: past, present, and prospect, Prog. Biophys. Mol. Biol. (2003) 3–9, https://doi.org/10.1016/S0079-6107(03)00022-1.

[33] K. Nakano, N. Nanri, Y. Tsukamoto, M. Akashi, Mechanical activities of self-beating cardiomyocyte aggregates under mechanical compression, Sci. Rep. 2021 111 (11) (2021) 1–10, https://doi.org/10.1038/s41598-021-93657-z.